Plasmon modes and screening in double metallic armchair graphene nanoribbons

Cesar E. P. Villegas and Marcos R. S. Tavares[*]

Centro de Ciências Naturais e Humanas, Universidade Federal do ABC, Santo André, SP 09210-170, Brazil

G.-Q. Hai

Instituto de Física de São Carlos, Universidade de São Paulo, São Carlos, SP 13560-970, Brazil

P. Vasilopoulos

Concordia University, Department of Physics, 7141 Sherbrooke Ouest, Montreal, Quebec, Canada H4B 1R6

We theoretically study the plasmon modes in double parallel metallic armchair graphene nanoribbons (AGNRs) separated by a distance L_b. Starting with a single *doped* metallic AGNR *at zero temperature*, we show the plasmon dispersion dependence on the Fermi wave vector. By evaluating the static dielectric function for this ribbon, we find that the usual logarithmic divergence at $q = 2k_F$ is absent. This indicates that plasmons in metallic AGNRs might be the most robust charge-density oscillations occurring in quasi-one-dimensional electron systems. We also study the influence of the distance L_b and of the carrier densities on the out-of-phase and in-phase plasmon modes. Finally, we address the intra-intersubband electron-hole transitions in single metallic armchair ribbons and find a strong influence of doping on the intrasubband plasmon modes.

PACS number(s): 78.67.Wj, 73.22.Pr

I. INTRODUCTION

Graphene has drawn considerable attention due to its remarkable electronic properties[1] which arise as a direct consequence of the linear dispersion relation for energies near the Dirac points (valleys) **K** and **K**′. The high mobility of charges, high optical transmittance, and the easy way of tuning the carrier density are important features that should turn graphene into an excellent material for a wide variety of potential applications in electronics, plasmonics, and optoelectronics.[1–6] On the other hand, plasmons, which are collective or charge-density excitations, can be found in metals or in bulk materials and possess a wide applicability in improving some specific properties of metamaterials[7] and photovoltaic devices.[8] The interest in plasmons is a direct consequence of their capability to confine electromagnetic energy on nanometer scale[9] and thus increase the incident light intensity over the material. As a matter of fact, the plasmon oscillation in graphene, which is strongly related to the charge-carrier density, can be tuned in a wide range of frequencies on the THz scale.[10] This feature seems to be sufficient to produce high field confinement and long-lifetime plasmons.[11] Nevertheless, graphene-based nanostructures can offer further benefits with respect to the plasmons, such as strong plasmon localization and extremely high field confinement.[10] In this sense, nanopatterned samples of graphene, such as graphene nanoribbons (GNRs), are promising systems and worth further exploration.

The GNRs, made by cutting the graphene sample in strips a few nanometers wide, have different electronic properties than the bulk graphene, especially with regard to the strong dependence on the crystallographic orientation,[12] the type of edge termination,[13] and the ribbon width.[14] In fact, plasmons on graphene-based nanostructures have been widely investigated but most of these investigations rely on a classical electromagnetic description.[15–18] A quantum treatment of plasmons in some graphene nanostructures has been carried out[19–23] but only two pertain to single graphene nanoribbons.[19,22]

Accordingly, further investigations concerning, for instance, intersubband electron-hole transitions and especially two parallel interacting GNRs could provide additional insights and lead to potential new applications.

In this paper we study the plasmon modes and the dielectric properties of metallic armchair graphene nanoribbons (AGNRs) within the random-phase approximation (RPA).[24] Three configurations of AGNRs are studied in detail: (i) undoped and doped metallic AGNRs, (ii) two parallel metallic AGNRs, (iii) doped metallic AGNRs. In (i) and (ii) only the lowest subband in the conduction band is occupied while in (iii) the lowest and first excited state in the conduction band are occupied. Our results show that within the long-wavelength limit the plasmons in doped metallic AGNRs disperse as $(2k_F q + q^2)^{1/2}\sqrt{|\ln qL|}$, and the static dielectric function for these ribbons does not present the usual logarithmic divergence at $q = 2k_F$. This allows us to surmise that plasmons in metallic AGNRs might be the most robust carrier density oscillations occurring in quasi-one-dimensional (Q1D) systems. Furthermore, when considering double metallic AGNRs, separated by a distance L_b and having the same carrier densities, the in-phase and out-of-phase plasmon modes become degenerate as L_b increases. Moreover, by considering different carrier densities in the ribbons, we observe that the in-phase mode becomes more robust whereas the out-of-phase mode is sensitive to the doping. Finally, we study the intra-intersubband electron-hole transitions in metallic armchair ribbons where our results show a strong influence of doping on the intrasubband plasmon mode.

The paper is organized as follows. In Sec. II we present the electronic structure of a single AGNRs. In Sec. III we present the theoretical formalism and the main results for the dielectric function and the screening properties of doped metallic AGNRs and double parallel metallic AGNRs. The results are elucidated with several pertinent figures. Finally, in Sec. IV we present our conclusions and in the appendixes some details for the calculation of the polarizabilities.
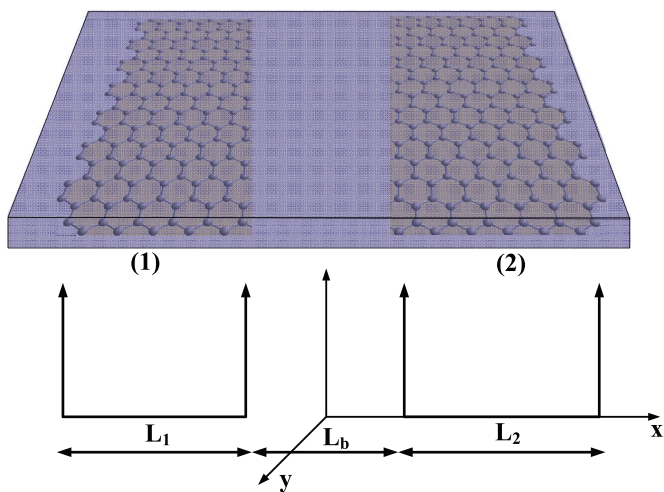
FIG. 1. (Color online) Schematic representation of two parallel armchair graphene nanoribbons. L_1 and L_2 are the widths of the ribbons and L_b is the separation between them.

II. ELECTRONIC STRUCTURE

We focus our attention on a single GNR with armchair edges, infinitely extended in the y direction and with finite width $L = (N-1)\sqrt{3}a/2$ in the x direction. N is an integer number which is properly chosen to define the metallic or semiconductor character of the ribbon, and $a = 0.142$ nm is the lattice parameter. Such a system can be obtained from Fig. 1 by considering $L_b = 0$ and $L = L_1 + L_2$. Within the low-lying energy limit near the Dirac points $\mathbf{K} = (4\pi/3\sqrt{3}a)(1,0)$ and $\mathbf{K}' = (4\pi/3\sqrt{3}a)(-1,0)$, the quantum states of AGNRs can be combined into a four-component spinor $\Psi = [\psi_A(\mathbf{r}), \psi_B(\mathbf{r}), \psi_A'(\mathbf{r}), \psi_B'(\mathbf{r})]^T$, where the superscript T indicates the transpose. These spinors are eigenvectors of the Hamiltonian

$$H = \gamma \begin{bmatrix} \sigma \cdot \mathbf{k} & 0 \\ 0 & -\sigma^* \cdot \mathbf{k} \end{bmatrix}, \qquad (1)$$

where $\gamma = 0.593$ nm eV, $\mathbf{k} = (k_x, k_y)$ is the wave vector, and $\sigma = (\sigma_x, \sigma_y)$ is the 2D Pauli vector.

For an AGNR the boundary conditions at the edges demand the vanishing of the wave-function components at points $x = 0$ and $x = L$. Due to the translational invariance in the y direction, the wave function for an AGNR can be written as

$$\Psi(x,y) = \frac{e^{ik_y y}}{2\sqrt{LL_y}} \begin{bmatrix} se^{-i\theta_{k_n}} e^{ik_n x} \\ e^{ik_n x} \\ -se^{-i\theta_{k_n}} e^{-ik_n x} \\ -e^{-ik_n x} \end{bmatrix}, \qquad (2)$$

where

$$k_n = n\pi/L - 4\pi/(3\sqrt{3}a) \qquad (3)$$

is the wave vector of the nth subband, $s = +(-)$ is the usual band index for graphene's band, and $\theta_{k_n} = \arctan(k_y/k_n)$ expresses the coupling between k_y and k_n. The corresponding eigenvalue is $E_n^s = s\gamma[k_n^2 + k_y^2]^{1/2}$. Note that while the condition $N = 3m - 1$, $m \in Z$ is satisfied, the band structure of the

ribbon describes a semimetallic material. Otherwise, the band structure of the ribbon possesses an energy gap.

III. COLLECTIVE EXCITATIONS

Within the RPA and considering the charge-density oscillations in the y direction, the dielectric matrix for an AGNR can be written as[24]

$$\epsilon_{ijmn}(q,\omega) = \delta_{im}\delta_{jn} - \upsilon_{ijmn}(q)\Pi_{mn}(q,\omega), \qquad (4)$$

where i, j, m, and n are the indices for subbands. $\Pi_{mn}(q,\omega)$ is the 1D polarizability given by

$$\Pi_{mn}(q,\omega) = g_s \sum_{k_y, s, s'} \frac{f[E_m^s(k_y + q)] - f[E_n^{s'}(k_y)]}{E_m^s(k_y + q) - E_n^{s'}(k_y) - \hbar\omega}$$
$$\times F^{ss'}(k_y, k_y + q), \qquad (5)$$

where $s, s' = 1\,(-1)$ are the indices related to the conduction (valence) band, g_s is the spin degeneracy, and $f(E)$ is the Fermi distribution function. $E_n^\pm = \pm\gamma(k_n^2 + k_y^2)^{1/2}$ are the eigenvalues of the system and $F^{ss'}(k_y, k_y + q)$ is the overlap of states with value

$$F^{ss'}(k_y, k_y + q) = (1 + ss'\cos\theta)/2; \qquad (6)$$

here θ is the angle between (k_n, k_y) and $(k_n, k_y + q)$. Following a procedure similar to that commonly used in literature,[20,25,26] we perform the summations over s and s'. Then we can rewrite the polarizability as the sum of the contribution from doped and undoped cases,

$$\Pi_{mn}(q,\omega) = \Pi_{mn}^0(q,\omega) + \Pi_{mn}^1(q,\omega), \qquad (7)$$

where $\Pi_{mn}^0(q,\omega) = -\chi_{mn,\infty}^-(q,\omega)$ is the polarizability of only interband transitions, corresponding to the undoped case ($E_F = 0$), and $\Pi_{mn}^1(q,\omega) = \chi_{mn,\mu}^+(q,\omega) + \chi_{mn,\mu}^-(q,\omega)$ is the polarizability of the intraband and interband transitions, corresponding to the doped case ($E_F > 0$). *At zero temperature,* the full expression for each polarizability term can be written as

$$\chi_{mn,D}^\pm(q,\omega)$$
$$= \frac{g_s}{2\pi} \int dk_y \left[\frac{1}{\mp E_m(k_y + q) + E_n(k_y) + \hbar\omega + i\delta} \right.$$
$$\left. - \frac{1}{\pm E_m(k_y + q) - E_n(k_y) + \hbar\omega + i\delta} \right] F^\pm(k_y, k_y + q). \qquad (8)$$

Note that the superscripts $+(-)$ refer to intraband and interband electron-hole transitions, respectively, and the parameter D defines the integration limits. On the other hand, the Coulomb matrix elements are given by

$$\upsilon_{ijmn}(q) = \frac{2e^2}{\epsilon_0 L^2} \int dx' \int dx\, K_0(q|x - x'|)$$
$$\times \cos(k_i - k_j)x \cos(k_m - k_n)x', \qquad (9)$$

where k_i, defined in Eq. (3), is the quantized wave vector in the transverse direction for the ith subband and K_0 is the modified Bessel function of the second kind. We point out that the RPA might be improved straightforwardly to include local-field corrections. This has been done for bulk graphene.[27]
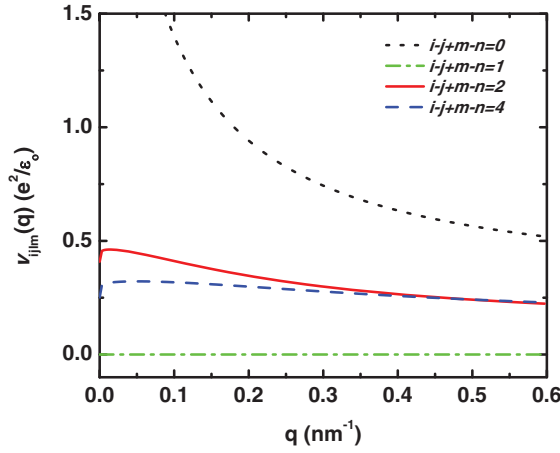
FIG. 2. (Color online) Coulomb potential matrix elements, in units of e^2/ϵ_0, as a function of the transferred wave vector q for a single metallic AGNR of width $L = 18.4$ nm.

Before we proceed further we analyze the relevant elements of the Coulomb potential matrix. In Fig. 2 we present the four Coulomb matrix elements as a function of the transferred wave vector q. As can be noticed, due to the presence of harmonic functions in Eq. (9), the Coulomb potential matrix possesses vanishing elements when the sum $i - j + m - n$ is an odd integer as the green dash-dotted line shows. The more relevant transitions, indicated by the black dashed and red solid curves, satisfy the condition $i - j + m - n = 0, 2$, respectively. As a matter of fact, the condition $i - j + m - n = 0$ corresponds to intrasubband electron-hole transitions, whereas the condition $i - j + m - n = 2$ corresponds to intersubband electron-hole transitions. Because these transitions are the most relevant in the system, we focus this study on describing a two-subband model for the dielectric function. It is worth mentioning that after performing the summation over s, s', the subindices of the dielectric matrix can represent both the subband index and the ribbon index. Thus, the theoretical formalism used in this work is valid for describing inter-ribbon transitions as well as intersubband transitions. If we desire to describe two parallel metallic AGNRs, then the subindices of the dielectric matrix assume the values $i = j = m = n = 1, 2$. Accordingly, the determinant of the dielectric matrix can be written as

$$
\begin{aligned}
\det \epsilon(q, \omega) = {} & [(1 - \upsilon_{1111}\Pi_{11})(1 - \upsilon_{2222}\Pi_{22}) - \upsilon_{1122} \\
& \times \upsilon_{2211}\Pi_{11}\Pi_{22}][(1 - \upsilon_{1212}\Pi_{12})(1 - \upsilon_{2121}\Pi_{21}) \\
& - \upsilon_{1221}\upsilon_{2112}\Pi_{21}\Pi_{12}],
\end{aligned}
\tag{10}
$$

and the plasmon modes are given by the zeros of this determinant. Before studying the plasmon modes of two interacting AGNRs, we investigate those of a single metallic AGNR with only the lowest subband occupied by electrons.

A. Single armchair graphene nanoribbon at zero temperature

First, we consider an undoped metallic AGNR of width L, in which only interband transitions are allowed. Thus, we focus on plasmons that occur near the lowest subband (linear dispersion relation). Because we are dealing with a single AGNR, the polarizabilities $\Pi_{22} = \Pi_{21} = \Pi_{12}$ vanish so the determinant in Eq. (10) is reduced to the expression
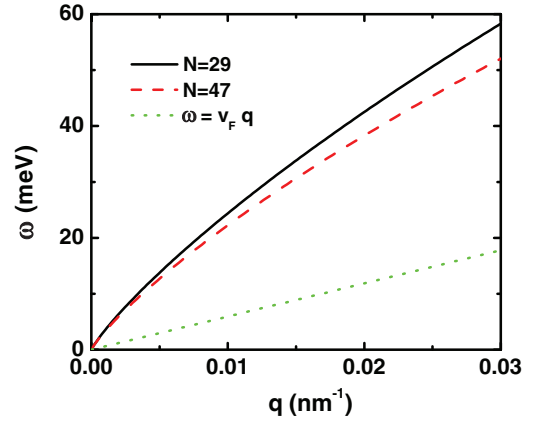
FIG. 3. (Color online) The plasmon mode of an undoped metallic AGNR for two different widths $L = 28\sqrt{3}a/2$ (solid line) and $L = 46\sqrt{3}a/2$ (dashed line). The SPE is indicated by the green dotted line and governed by the equation $\hbar\omega = \gamma q$.

$\det \epsilon(q, \omega) = (1 - \upsilon_{1111}\Pi_{11}^0)$. In order to obtain the plasmon modes, we begin by calculating the imaginary part of the polarizability given by

$$
\begin{aligned}
\text{Im}\,\Pi_{11}^0 = {} & - \int dk_y[\delta(-E_{k_y+q} - E_{k_y} + \hbar\omega) \\
& - \delta(E_{k_y+q} + E_{k_y} + \hbar\omega)]F^-(k_y, k_y + q).
\end{aligned}
\tag{11}
$$

It can be noticed that $F^-(k_y, k_y + q)$ is responsible for the absence of backscattering in undoped AGNRs. As a matter of fact, it can be shown that for the lowest subband energy the overlap of states satisfies the condition $F^-(k_y, k_y + q) = 1$.[22] Using this condition and the Kramer-Kronig relations we obtain, cf. Appendix A, the real part of the polarizability

$$
\text{Re}\,\Pi_{11}^0 = \frac{1}{\gamma}\ln\left(\frac{\hbar\omega/\gamma + q}{\hbar\omega/\gamma - q}\right).
\tag{12}
$$

In Fig. 3 we show the plasmon dispersion for an undoped metallic AGNR ($E_F = 0$) with different widths $\propto N$. It can be noticed that as the width is increased the plasmon energy is reduced. The green dotted line, which follows the law $\hbar\omega = \gamma q$, represents the electron-hole continuum also known as single-particle excitations (SPEs), i.e., the region where the fluctuations of the charge-density dissipate. As a matter of fact, due to the singular character of Eq. (12), in general, for long values of q the plasmon energy $\hbar\omega$ tends to γq, but in reality it should satisfy the condition $\hbar\omega \neq \gamma q$. Furthermore, by considering the long-wavelength limit ($q \to 0$) we find that the plasmon dispersion becomes $\hbar\omega \approx [(4e^2\gamma/\pi\epsilon_0)q^2|\ln(qL)|]^{1/2}$, which agrees with the result of previous calculations.[19]

Next, we consider a n-doped metallic AGNR ($E_F > 0$). Notice that for this case both interband and intraband transitions are allowed. For the sake of simplicity, in this calculation we neglect the intersubband electron-hole transitions. Thus, we assume that the plasmon oscillation takes place near the Fermi level which is above only the lowest subband (linear dispersion). From Eq. (7) it can be noticed that by calculating the polarizability Π_{11}^1 we are able to find the plasmon modes. Indeed, for a doped metallic AGNR *at zero temperature*, the polarizability can be found in a straightforward manner
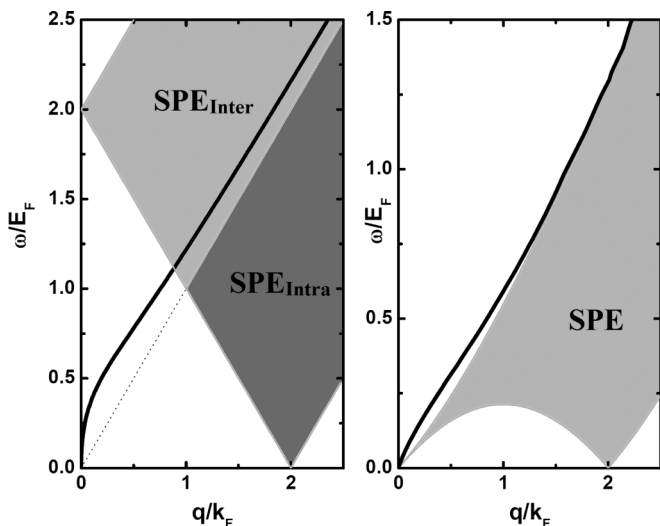
FIG. 4. Left panel: Plasmon dispersion for a doped AGNR with $L = 73\sqrt{3}a/2$ and carrier density $n = 1 \times 10^6$ cm^{-1}. Right panel: The plasmon dispersion and the SPE (shaded area) for a conventional Q1D system with quadratic dispersion relation.

without using the Kramer-Kronig relations. By evaluating the integral in Eq. (8) and considering only nonzero values of the overlap $F^{\pm}(k_y, k_y + q)$, we find

$$\mathrm{Re}\, \Pi_{11}^1 = \frac{g_s}{2\pi\gamma}\left(\frac{2k_F q}{(\hbar\omega/\gamma)^2 - q^2}\right).$$ (13)

On the other hand, the imaginary part of Π_{11}^1 can be obtained if we use, without any essential limitation, the condition $F^{\pm}(k_y, k_y + q) = 1$. The result is

$$
\begin{aligned}
\mathrm{Im}\, \Pi_{11}^1 = {} & -\frac{1}{\gamma}\Theta(q - \omega)\left[\Theta\left(k_F - \frac{\hbar\omega/\gamma + q}{2}\right)\right. \\
& \left. - \Theta\left(k_F - \frac{q - \hbar\omega/\gamma}{2}\right)\right] + \frac{1}{\gamma}\Theta(\omega - q) \\
& \times \left[\Theta\left(\frac{\hbar\omega/\gamma - q}{2}\right) - k_F\right. \\
& \left. - \Theta\left(\frac{\hbar\omega/\gamma + q}{2}\right) - k_F\right].
\end{aligned}
$$ (14)

In the left panel of Fig. 4 we present the plasmon dispersion (black solid line) calculated by using the condition $1 - \upsilon_{1111}(\Pi_{11}^1 + \Pi_{11}^0) = 0$ for a metallic AGNR with parameters $k_F = 0.15$ nm^{-1} and $N = 74$. If we consider the long-wavelength limit, we find that the plasmon mode takes the form $\hbar\omega \approx [(4e^2\gamma/\pi\epsilon_0)(2k_F q + q^2)\,|\ln(qL)|]^{1/2}$. This result shows that, *at zero temperature*, the plasmon mode *in doped* metallic AGNR depends on the carrier density ($n = 2k_F/\pi$). Besides, the shaded regions indicate the electron-hole continuum, where Landau damping takes place. The lower region, where intraband transitions are available, is bounded by the curves $\gamma q - 2E_F < \hbar\omega < \gamma q$ and $\hbar\omega > 2E_F - \gamma q$. On the other hand, the upper region, where interband transitions are allowed, is delimited by the curves $\gamma q + 2E_F > \hbar\omega > \gamma q e \hbar\omega > 2E_F - \gamma q$. Note that with q in the interval $\in [0, 2k_F]$ and for $\omega = 0$, the SPE does not exist. This is a direct consequence of the 1D confinement and the
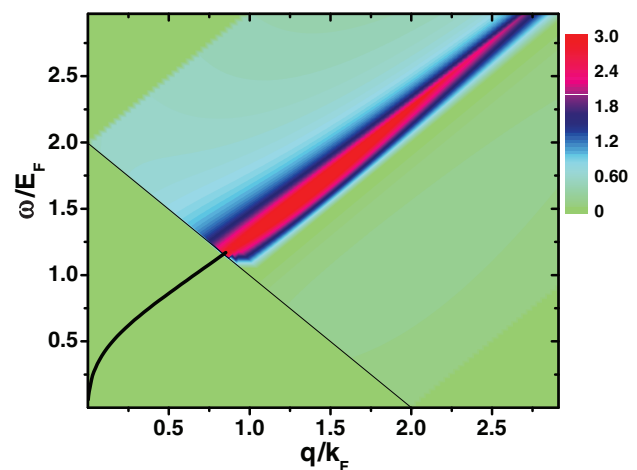
FIG. 5. (Color online) Contour plot of the spectral loss function vs the energy ω and wave vector q. The AGNR has a width $L = 73\sqrt{3}a/2$ and a carrier density $n = 2.3 \times 10^6$ cm^{-1}.

linear relation dispersion. Moreover, it can also be observed that the point $(k_F, \hbar\omega)$ corresponds to the minimum energy for which intersubband transitions take place in the system. In order to compare the space phase ω-q of our Q1D system, in the right panel of Fig. 4 we show the plasmon dispersion and the SPE for a conventional Q1D electron gas based on GaAs semiconductor with parabolic dispersion $E = \hbar^2 k^2/2m$.[28] In a conventional Q1D system for $\omega = 0$ and q in the interval $\in [0, k_F]$, there exists a gap which is closely related to the perfect nesting of the Fermi surface in 1D systems. From the left panel of Fig. 4 we notice that the plasmon mode enters the intersubband SPE where it is expected to be damped. In order to observe such a behavior we study the spectral loss function

$$S(q, \omega) = -\mathrm{Im}[\epsilon^{-1}(q, \omega)],$$ (15)

which quantifies the Landau damping of the system. In fact, this function can be measured by experimental techniques such as inelastic electron spectroscopy. Accordingly, in Fig. 5 we plot the loss function versus the energy ω and the transferred wave vector q. Because the plasmon mode satisfies the condition $\hbar\omega > \gamma q$, we expect a damping of this mode by the interband SPE. The plasmon mode enters into the interband SPE at a given $\omega(q_c) = 2E_F - \gamma q_c$ and decays by emitting electron-hole pairs. Then for $q > q_c$ the plasmon mode is damped as shown in Fig. 5. The red color in the damping region expresses the decay of the plasmon mode which is much weaker than in 2D graphene.[26] At this moment we should emphasize that the results shown in Fig. 5 are obtained using the condition $F^{ss'}(k_y, k_y + q) = 1$. Nevertheless, a detailed inspection of the real part of Π_{11}^1 and of the overlap $F^{ss'}(k_y, k_y + q)$ (see Appendix B) allows us to conclude that despite the fact that the interband and intraband SPE are well-defined regions, there is a possibility of finding, in Eq. (8), certain ranges of k_y values that could effectively make the overlap of states vanish and, as a consequence, the SPE regions, shown in Fig. 4(a), to be dramatically reduced into a single line given by $\hbar\omega = \gamma q$, which is exactly the same SPE of the undoped case. Thus, henceforth the SPE for doped AGNRs is represented by the relation $\hbar\omega = \gamma q$. We believe the plasmon branches shown in the present work can provide
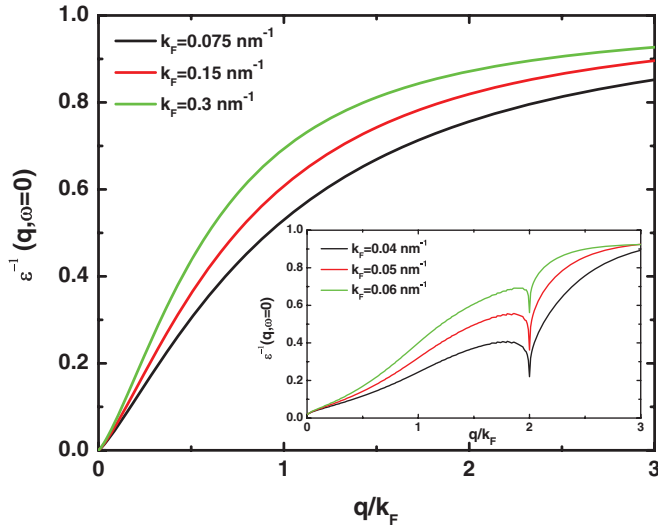
FIG. 6. (Color online) The inverse static dielectric response function versus the transferred wave vector q for a doped metallic AGNR with different Fermi wave vectors. The with of the AGNR is $L = 73\sqrt{3}a/2$. Inset: The same function but for a doped semiconductor AGNR of width $L \approx 15$ nm.

the same features as those in Ref. 29 if the electron-electron correlation (or self-energy calculation) is taken into account.

1. Static screening

We now study the static dielectric properties of a single metallic AGNR. For this purpose, we consider an external charge density, $n_0 = Ze\delta(\mathbf{r})$, screened by free electrons. Then the induced charge density can be written as

$$\delta_n(r) = \frac{Ze}{2\pi} \int dq \, [\epsilon^{-1}(q,0) - 1]e^{iqr}. \quad (16)$$

With this expression we are able to study the induced charge density as a function of the distance r. We begin by studying the static dielectric function. Note that we are dealing here with a single ribbon with one occupied subband, so that the dielectric function is no longer a tensor. In Fig. 6 we show the inverse dielectric function, $\epsilon^{-1}(q,\omega = 0)$, as a function of the transferred wave vector q for different carrier densities (Fermi wave vectors). As the n doping in the system is increased, the inverse of the static dielectric function increases rapidly to 1. This result indicates that the screening in the Q1D electron gas increases with the Fermi wave vector. Thus, one might understand that more induced impurities arise in the system as a direct consequence of increasing the doping. The inset shows the same function describing a semiconductor AGNR. Notice that the doping in this new system induced similar effects as in the metallic case. However, in metallic AGNRs the logarithmic singularity at $q = 2k_F$, a principal characteristic of Q1D systems, is absent. In fact, such a singularity should arise as a direct consequence of the perfect nesting of the Fermi surface and is associated with the stability of the system. Here, it is absent and such an unexpected phenomenon suggests that at zero temperature, the plasmon oscillations in metallic AGNRs might be more robust than those in semiconductor AGNRs. This result allow us to suggest
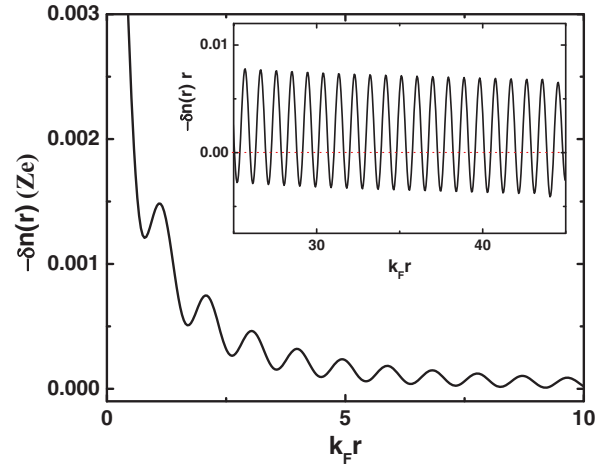
FIG. 7. (Color online) Induced charge density, as a function of the distance, for a AGNR with carrier density $n = 1 \times 10^6$ cm^{-1} and width $L = 73\sqrt{3}a/2$. The inset shows how the charge density changes sign for large distances.

that designing plasmonic devices based on metallic AGNRs may provide more stable devices which are free from the Fermi edge singularities.

For the sake of completeness in Fig. 7 we present the induced charge-density fluctuations as a function of the distance r. It can be noticed that as the charge density is away from the impurity the density oscillations are reduced rapidly. We also notice that the density fluctuations for values in the range $k_F r < 15$ do not change sign. On the other hand, for $k_F r > 15$ the induced density fluctuations change sign. This behavior is shown in the inset. It is worth mentioning that the Friedel oscillations period in metallic AGNRs is similar to that in conventional Q1D semiconductor systems. However, we notice that they decay faster in AGNRs.[30]

B. Double metallic graphene nanoribbons

In what follows we study the plasmon modes in double, parallel, and metallic AGNRs separated by a distance L_b, as shown in Fig. 1. Because the wave functions outside the nanoribbons vanish, there is no tunneling between the ribbons, so the polarizabilities should be $\Pi_{21} = \Pi_{12} = 0$. We mention that the subscripts in the polarizabilities should be understood as ribbon indices (see Fig. 1). Indeed, we assumed that the plasmons oscillations take place only near the Fermi level that lies in the lowest subband. Then Eq. (10) takes the simpler form

$$\epsilon(q,\omega) = (1 - \upsilon_{1111}\Pi_{11})(1 - \upsilon_{2222}\Pi_{22})$$
$$- \upsilon_{1122}\upsilon_{2211}\Pi_{11}\Pi_{22}. \quad (17)$$

In order to obtain the plasmon modes of the system we set the carrier density as $n_1 = n_2 = 2k_F/\pi$, with $k_F = 0.15$ nm^{-1}. In Fig. 8 we plot the plasmon modes $\omega^{\pm}$ for different values of the distance L_b. In the four figures the SPE is given by the curve $\hbar\omega = \gamma q$. The upper left panel of Fig. 8 is for a short separation between the metallic AGNRs ($k_F L_b < 1$) for which the frequency of the out-of-phase plasmon mode ω^- is very close to the SPE. On the other hand, the in-phase mode ω^+ is located far from the SPE. As a matter of fact, our results
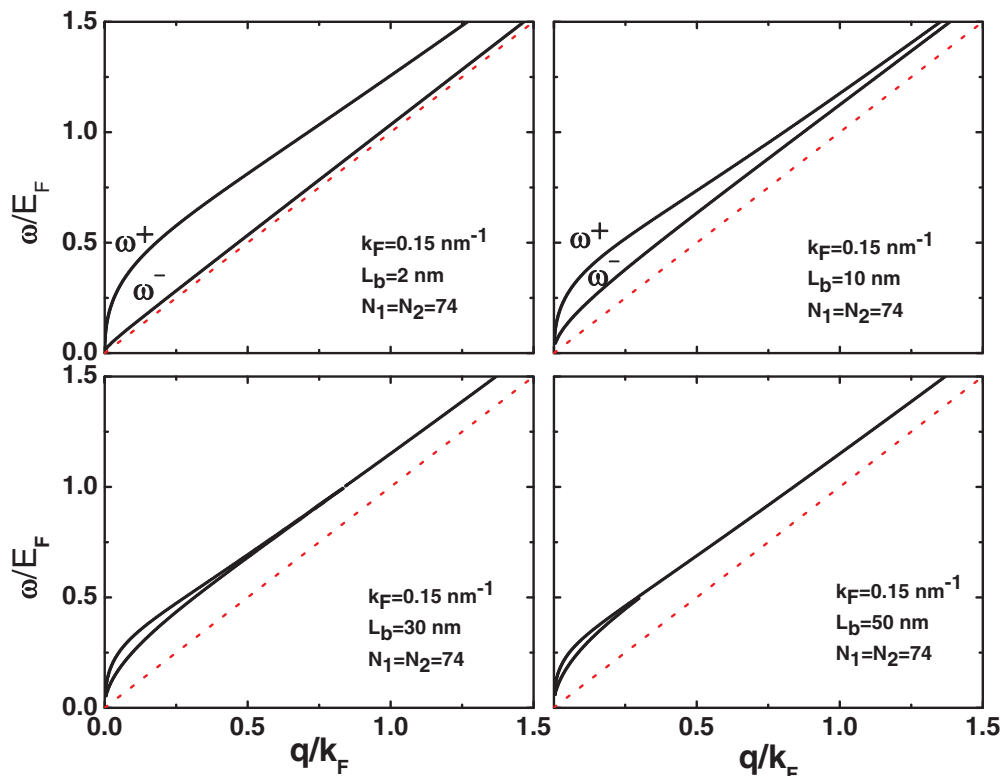
FIG. 8. (Color online) The out-of-phase ω^- and in-phase ω^+ plasmon modes of two parallel metallic AGNRs for different distances L_b with a fixed carrier density $n = 1 \times 10^6$ cm^{-1} and widths $L_1 = L_2 = 73\sqrt{3}a/2$. The dotted line represents the SPE that follows the equation $\hbar\omega = \gamma q$.

show that, as the distance $L_b \to 0$, the in-phase plasmon mode ω^- becomes degenerate with the SPE. In such a situation, the two parallel metallic AGNRs become a unique AGNR of width $2L$ and carrier density $n_1 + n_2$, where only the in-phase plasmon mode ω^+ exists. In addition, as the separation L_b, increases, the out-of-phase plasmon mode increases its amplitude and remains close to the in-phase mode. Indeed, our results show that in the limit, $L_b \to \infty$, the out-of-phase and in-phase modes become completely degenerate, i.e., a single in-phase plasmon mode. This limiting situation is equivalent to studying one metallic AGNR of width L and carrier density $n = n_1 = n_2$.

Furthermore, in Fig. 9 we analyze the plasmon modes by keeping fixed the distance $L_b = 10$ nm and considering different carrier densities in the metallic AGNRs ($n_1 \neq n_2$). We observe that, as the ratio n_2/n_1 decreases, the out-of-phase plasmon mode ω^- approaches rapidly the SPE, whereas the in-phase plasmon mode ω^+ does not seriously suffer from modifications associated to its intensity. Thus, the weak dependence of the in-phase mode on the ratio of the carrier densities might serve as a way to characterize the out-of-phase plasmon modes, which are more difficult to observe experimentally.

C. intra-intersubband e-h transitions

Finally, we investigate the plasmon modes in a single metallic AGNR when the Fermi level is above the first excited state of the conduction band. In this situation the transitions between

these subbands are relevant and the polarizabilities Π_{12} and Π_{12} possess nonvanishing values. It is worth mentioning that because our study is focused on transitions between subbands of the conduction band, we label this kind of excitations intra-intersubband electron-hole transitions that should not be confused with interband transitions. Then the plasmon modes of the system can be found from Eq. (10). In order to make
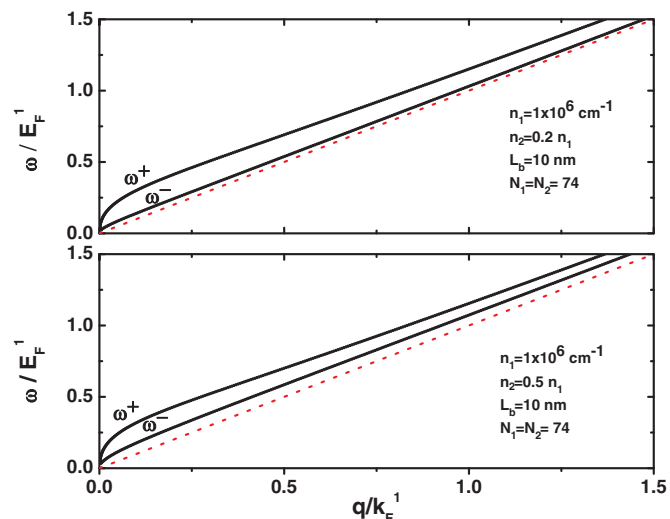
FIG. 9. (Color online) The same phase space for two parallel metallic AGNRs for different carrier densities ($n_1 \neq n_2$) but the same inter-ribbon distance L_b and ribbon widths.
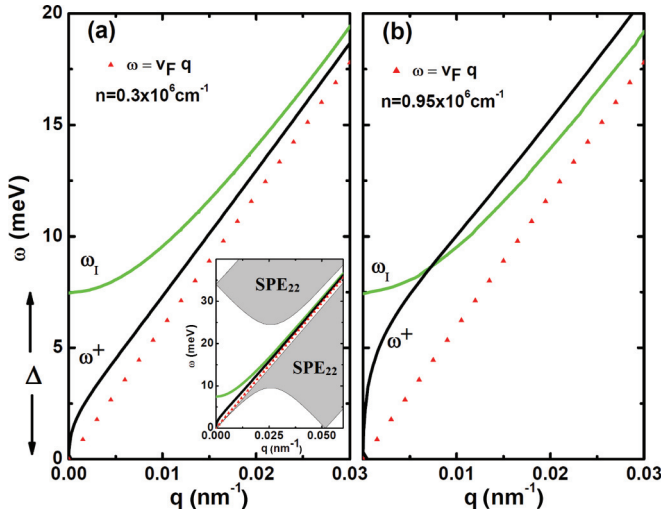
FIG. 10. (Color online) Plasmon modes for (a) $n = 0.3 \times 10^6$ cm^{-1} and (b) $n = 0.95 \times 10^6$ cm^{-1}. The modes ω_I and ω^+ is the intra-intersubband and optical modes, respectively. The inset shows the electron-hole continuum (SPE) associated with intra-subband transitions in the first excited state (hyperbolic dispersion relation).

the intra-intersubband transitions of the system significant, we must consider a system where the lowest and the first excited subbands are very close. This can occur if we consider a metallic AGNR of considerable width. Thus, we set the width of the ribbon to $L = 2033\sqrt{3}a/2$. Then the energy gap between the lowest subband and the first excited subband is $\Delta = 7.41$ meV. This case is interesting to investigate because the two different electronic states with different dispersions (linear and hyperbolic) are interacting. In Fig. 10 we show the plasmon modes for different dopings. The mode ω^+ is closely related to the intra-intrasubband transitions (polarizabilities Π_{11} and Π_{22}) whereas the plasmon mode ω_I is associated to the intra-intersubband transitions (polarizabilities Π_{21} and Π_{12}). Furthermore, as a direct consequence of the intra-intrasubband polarizabilities, we find another plasmon mode ω^- not shown in Fig. 10 for the sake of simplicity. As a matter of fact, our results show that this mode becomes completely degenerate with the SPE ($\hbar\omega = \gamma q$) related to the polarizability Π_{11}. Moreover, as the doping increases the mode ω^+ is strongly modified, while the mode ω_I remains more robust to the doping effects. In the inset we show the SPE related to the first excited state (the one with hyperbolic dispersion). Note that both modes are damped by this SPE associated with the first subband. This results suggest that the intra-intrasubband plasmon mode of a two-subband model can be used for improving plasmonic devices.

IV. CONCLUSIONS

We theoretically studied the plasmon modes and dielectric properties of metallic armchair graphene nanoribbons within the RPA and at zero temperature. We found that in a single doped metallic AGNR and in the long-wavelength limit the plasmon mode disperses as $[(2k_F q + q^2)\,|\ln qL|]^{1/2}$. We also studied the static dielectric function and found that the logarithmic divergence at $q = 2k_F$, the main feature

of Q1D systems, is absent. This fact allows us to suggest that plasmons in metallic AGNRs might be the most robust density oscillation occurring in Q1D systems. Furthermore, in double parallel AGNRs with the same doping the optical and acoustical plasmon modes become degenerate as the distance L_b increases. In addition, we addressed the intra-intersubband electron-hole transitions in metallic armchair ribbons and showed a strong influence of doping on the intra-intrasubband plasmon mode. Finally, we mention that our results could serve as a starting point for designing plasmonic devices based on waveguides armchair graphene nanoribbons.

APPENDIX A: UNDOPED NANORIBBONS AT ZERO TEMPERATURE

For undoped graphene nanoribbons the imaginary part of the polarizability is given by

$$\text{Im}\,\Pi_{11}^0 = -\int dk_y [\delta(-E_{k_y+q} - E_{k_y} + \hbar\omega) - \delta(E_{k_y+q} + E_{k_y} + \hbar\omega)]F^-(k_y, k_y+q). \quad \text{(A1)}$$

Performing the integral over k_y, $-k_c \leqslant k_y \leqslant k_c$, we obtain

$$\text{Im}\,\Pi_{11}^0 = -\frac{\pi}{\gamma}\,\Theta(\omega - q) \\ \times \left[\Theta\left(\frac{\hbar\omega/\gamma + q}{2} - k_c\right) \\ - \Theta\left(\frac{\hbar\omega/\gamma - q}{2} - k_c\right)\right]. \quad \text{(A2)}$$

On the other hand, with the help of the Kramer-Kronig relations, the real part of the polarizability can be written as

$$\text{Re}\,\Pi_{11}^0 = \frac{1}{\gamma}\ln\left(\frac{\hbar\omega/\gamma + q}{\hbar\omega/\gamma - q}\right). \quad \text{(A3)}$$

APPENDIX B: DOPED NANORIBBONS AT ZERO TEMPERATURE

Starting with Eq. (7) the real part of the polarizability is

$$\Pi_{11}^1(q,\omega) = \frac{g_s}{2\pi}\int dk_y\left[\frac{1}{-E_{k_y+q}^1 + E_{k_y}^1 + \hbar\omega}\right. \\ \left. - \frac{1}{E_{k_y+q}^1 - E_{k_y}^1 + \hbar\omega}\right]F^+(k_y, k_y+q) \\ + \int dk_y\left[\frac{1}{E_{k_y+q}^1 + E_{k_y}^1 + \hbar\omega}\right. \\ \left. - \frac{1}{-E_{k_y+q}^1 - E_{k_y}^1 - \hbar\omega}\right]F^-(k_y, k_y+q). \quad \text{(B1)}$$

This expression can be simplified by noting

$$\frac{1}{-E^1_{k_y+q} + E^1_{k_y} + \hbar\omega} - \frac{1}{E^1_{k_y+q} - E^1_{k_y} + \hbar\omega} = \frac{2\Delta_k}{(\hbar\omega)^2 - \Delta_k^2},$$
(B2)

$$\frac{1}{E^1_{k_y+q} + E^1_{k_y} + \hbar\omega} - \frac{1}{-E^1_{k_y+q} - E^1_{k_y} - \hbar\omega} = \frac{2\Delta'_k}{(\hbar\omega)^2 - \Delta_k'^2},$$
(B3)

where $\Delta_k = \gamma |k_y + q| - \gamma |k_y|$ and $\Delta'_k = \gamma |k_y + q| + \gamma |k_y|$. Thus, the polarizability can be rewritten as

$$\Pi^1_{11}(q,\omega) = \frac{g_s}{2\pi} \left[\int_{-k_F}^{k_F} dk_y \frac{2\Delta_k}{(\hbar\omega)^2 - \Delta_k^2} F^+(k_y, k_y + q) \right. $$
$$\left. + \int_{-k_F}^{k_F} dk_y \frac{2\Delta'_k}{(\hbar\omega)^2 - \Delta_k'^2} F^-(k_y, k_y + q) \right].$$
(B4)

Notice that the angle of scattering $\theta_{k_y,k_n} = \arctan(k_y/k_n)$ for a linear dispersion, i.e., for $k_n = 0$, can only take the following values:

$$\theta_{k_y,k_n} = \begin{cases} \pi/2; & k_y > 0, \\ -\pi/2; & k_y < 0. \end{cases}$$
(B5)

Consequently, the overlap of states $F^{\pm}(k_y, k_y + q) = [1 \pm \cos(\theta_{k_y+q,k_n} - \theta_{k_y,k_n})]/2$ for interband transitions takes the values

$$F^-(k_y, k_y + q) = \begin{cases} 1; k_y + q > 0 \wedge k_y < 0, \\ 0; k_y + q > 0 \wedge k_y > 0, \\ 1; k_y + q < 0 \wedge k_y > 0, \\ 0; k_y + q < 0 \wedge k_y < 0. \end{cases}$$
(B6)

Similar relations can be found for the intraband transitions. Then, considering that interband transitions scattered the particles in opposite directions and intraband transitions scattered the particles in the same direction, we obtain

$$\Delta_k = \gamma |k_y + q| - \gamma |k_y| = \gamma q, \; k_y + q > 0, \; k_y > 0, \quad \text{(B7)}$$

$$\Delta'_k = \gamma |k_y + q| + \gamma |k_y| = \gamma q, \; k_y + q > 0, \; k_y < 0. \quad \text{(B8)}$$

Using Eqs. (B7) and (B8) we have

$$\Pi^1_{11}(q,\omega) = \frac{g_s}{2\pi} \int_{-k_F}^{k_F} dk_y \left[\frac{2\Delta_k}{(\hbar\omega)^2 - \Delta_k^2} F^+(k_y, k_y + q) \right.$$
$$\left. + \frac{2\Delta'_k}{(\hbar\omega)^2 - \Delta_k'^2} F^-(k_y, k_y + q) \right].$$
(B9)

Due to the values of the overlap of states for intraband and interband transitions, the integral $(0 \leqslant k_y \leqslant k_F)$ of the first term and that $(-k_F \leqslant k_y \leqslant 0)$ of the second term vanish; then the polarizability can be written as

$$\Pi^1_{11}(q,\omega) = \frac{2g_s}{\pi\gamma} \left[\frac{k_F q}{(\hbar\omega/\gamma)^2 - q^2} \right].$$
(B10)

The imaginary part of the polarizability, considering the full range of values of the overlap of states, can be obtained by making the change $\hbar\omega \to \hbar\omega + i\delta$ in Eq. (B10). Then we have

$$\Pi^1_{11}(q,\omega) = \frac{2g_s}{\pi\gamma} \left[\frac{k_F q}{(\hbar\omega/\gamma + i\delta)^2 - q^2} \right].$$
(B11)

Using the relation $1/(x + i\delta) = \text{P.V.}(1/x) - i\pi\delta(x)$, where P.V. stands for Principal Value and some algebra we obtain

$$\Pi^1_{11}(q,\omega) = \frac{2g_s}{\pi\gamma} \left[\frac{k_F q}{(\hbar\omega/\gamma)^2 - q^2} \right] - \frac{i 2 g_s k_F q}{\pi\gamma} \pi$$
$$\times \left[\frac{\delta(\hbar\omega/\gamma + q)}{\hbar\omega/\gamma - q} + \frac{\delta(\hbar\omega/\gamma - q)}{\hbar\omega/\gamma + q} \right]. \quad \text{(B12)}$$

The last two terms of Eq. (B12) clearly give us information about the imaginary part of the doped polarizability at zero temperature. Note that the Dirac δ functions $\delta(\hbar\omega/\gamma \pm q)$ indicate that the SPE is available only for $\hbar\omega = \gamma q$ or $\hbar\omega = -\gamma q$. Thus, we show that the SPE for doped metallic AGNRs (linear dispersion) follows the relation $\hbar\omega = \gamma q$ for positive energies. It is worth mentioning that Eq. (14) was obtained without any restriction on the overlap of states, i.e., by taking $F^{\pm}(k_y, k_y + q) = 1$ in Eq. (B1).

*marcos.tavares@ufabc.edu.br

[1] A. H. Castro Neto, F. Guinea, N. M. R. Peres, K. S. Novoselov, and A. K. Geim, Rev. Mod. Phys. **81**, 109 (2009).

[2] R. R. Nair, P. Blake, A. N. Grigorenko, K. S. Novoselov, T. J. Booth, T. Stauber, N. M. R. Peres, and A. K. Geim, Science **320**, 1308 (2008).

[3] K. S. Novoselov, A. K. Geim, S. V. Morozov, D. Jiang, Y. Zhang, S. V. Dubonos, I. V. Grigorieva, and A. A. Firsov, Science **306**, 666 (2004).

[4] A. K. Geim, Science **324**, 1530 (2009).

[5] A. N. Grigorenko, M. Polini, and K. S. Novoselov, Nat. Photon. **6**, 749 (2012).

[6] Q. Bao and K. P. Loh, ACS Nano **6**, 3677 (2012).

[7] V. M. Shalaev, Nat. Photon. **1**, 41 (2007).

[8] H. A. Atwater and A. Polman, Nat. Mater. **9**, 205 (2010).

[9] W. L. Barnes, A. Dereux, and T. W. Ebbesen, Nature (London) **424**, 824 (2003).

[10] L. Ju, B. Geng, J. Horng, C. Girit, M. Martin, Z. Hao, H. A. Bechtel, X. Liang, A. Zettl, Y. R. Shen, and F. Wang, Nat. Nanotechnol. **6**, 630 (2011).

[11] Pai-Yen Chen and Andrea Alù, ACS Nano **5**, 5855 (2011); M. Jablan, H. Buljan, and M. Soljačić, Phys. Rev. B **80**, 245435 (2009)

[12] V. Barone, O. Hod, and G. E. Scuseria, Nano Lett. **6**, 2748 (2006).

[13] M. Ezawa, Phys. Rev. B **73**, 045432 (2006).

[14] M. Y. Han, B. Özyilmaz, Y. Zhang, and P. Kim, Phys. Rev. Lett. **98**, 206805 (2007).

[15] A. Y. Nikitin, F. Guinea, F. J. Garcia-Vidal, and L. Martin-Moreno, Phys. Rev. B **84**, 161407 (2011).

[16] J. Christensen, A. Manjavacas, S. Thongrattanasiri, F. H. L Koppens, and F. J. García de Abajo, ACS Nano **6**, 431 (2012).

[17] A. A. Dubinov, V. Y. Aleshkin, V. Mitin, T. Otsuji, and V. Ryzhii, J. Phys.: Condens. Matter **23**, 145302 (2011).

[18] V. V. Popov, T. Yu. Bagaeva, T. Otsuji, and V. Ryzhii, Phys. Rev. B **81**, 073404 (2010).

[19] L. Brey and H. A. Fertig, Phys. Rev. B **75**, 125434 (2007).

[20] E. H. Hwang and S. Das Sarma, Phys. Rev. B **75**, 205418 (2007).

[21] X. F. Wang and T. Chakraborty, Phys. Rev. B **75**, 041404(R) (2007); **81**, 081402(R) (2010).

[22] D. R. Andersen, and H. Raza, Phys. Rev. B **85**, 075425 (2012).

[23] S. Thongrattanasiri, A. Manjavacas, and F. J. García de Abajo, ACS Nano **6**, 1766 (2012).

[24] G. D. Mahan, *Many Particle Physics*, 3rd ed. (Springer-Verlag, New York, 1990).

[25] L. Brey and H. A. Fertig, Phys. Rev. B **73**, 235411 (2006).

[26] B. Wunsch, T. Stauber, F. Sols, and F. Guinea, New J. Phys. **8**, 318 (2006).

[27] F. M. D. Pellegrino, G. G. N. Angilella, and R. Pucci, Phys. Rev. B **82**, 115434 (2010).

[28] M. R. S. Tavares, S. Das Sarma, and G.-Q. Hai, Phys. Rev. B **63**, 045324 (2001); M. R. S. Tavares, *ibid*. **71**, 155332 (2005).

[29] M. Polini, R. Asgari, G. Borghi, Y. Barlas, T. Pereg-Barnea, and A. H. MacDonald, Phys. Rev. B **77**, 081411(R) (2008).

[30] C. Bena, Phys. Rev. Lett. **100**, 076601 (2008).